Conference Proceedings

EuroSun 2014

Aix-les-Bains (France), 16 – 19 September 2014

A Multi-Functional Ventilated Façade model within a parallel and object-oriented numerical platform for the prediction of the thermal performance of buildings

Deniz Kizildag[1], Oriol Lehmkuhl[1,2], Joaquim Rigola[1] and Assensi Oliva[1]

[1]Centre Tecnològic de Transferència de Calor (CTTC)

Universitat Politècnica de Catalunya · BarcelonaTech (UPC),

ETSEIAT, C. Colom 11, 08222 Terrassa (Barcelona), Spain

Tel. +34-93-739.81.92, Fax: +34-93-738.89.20

cttc@cttc.upc.edu, http://www.cttc.upc.edu

[2]Termo Fluids S. L.

Magí Colet 8, 08024 Sabadell (Barcelona), Spain

termofluids@termofluids.com, http://termofluids.com

Abstract

The population growth, increasing demand for building services, higher levels of comfort requirements, and larger periods of time spent indoors are some of the main factors which indicate an upward energy consumption trend within the buildings of the industrialized countries in the coming years. Owing to this fact, there is a large potential for energy savings in the building sector, especially through the retrofitting of the existing buildings. Multi-functional ventilated façades have appeared as a possible solution in both new and retrofitted buildings in order to reduce the building energy demand. In addition to the improved thermal and acoustic behavior, the possibility of integrating innovative elements like photovoltaic modules or electrochromic devices make the multi-functional façades an interesting architectonic solution. Due to the widespread implementation of these innovative elements, there emerges a need for developing accurate tools and methodologies in order to analyze their performance. Thus, the present work aims at providing a numerical tool, which -linked with the capabilities of an existing numerical platform- can predict the thermal behavior of these elements. Its modular design permits the study of different façade configurations by replacing the actual standard elements with other innovative ones, considering different modes of operation and flow regimes in a versatile manner.

Key-words: Multi-Functional Ventilated Façade, Object-Oriented, Parallel Computation.

1. Introduction

Due to many factors like the population growth, increasing demand for building services, higher levels of comfort requirements, and larger periods of time spent indoors, energy consumption within the buildings can be considered currently as a key issue in overall energy consumption of industrialized countries. Moreover, this upward consumption trend is expected to grow in the coming years (Pérez-Lombard et al., 2008). Owing to this fact, there is a large potential for energy savings in the building sector, especially through the retrofitting of the existing buildings. Multi-functional ventilated façades have appeared as a possible solution in both new and retrofitted buildings in order to reduce the building energy demand. Besides the improved thermal behavior, a higher level of acoustic insulation, enhanced daylight illumination, or the possibility of integrating innovative elements like photovoltaic modules or electrochromic devices make the multi-functional façades an interesting architectonic solution. The widespread implementation of these elements in the new or retrofitted buildings, in parallel, stimulates the efforts in developing the necessary tools and methodologies for analyzing their performance.

Selection and/or peer review under responsibility of EuroSun2014 Scientific Committee
doi:10.18086/eurosun.2014.18.03 Available at http://proceedings.ises.org

The present work reports on the implementation of a multi-functional ventilated façade model within an existing parallel and object-oriented numerical platform for the prediction of the thermal performance of the buildings. To that end, a software module composed of a photovoltaic (PV) panel, a vertical natural convection channel element, and an opaque wall element is developed. The module presented here -linked with the capabilities of the existing NEST (Damle et al., 2011) numerical platform- is intended to be a useful tool to predict the thermal behavior of these innovative elements.

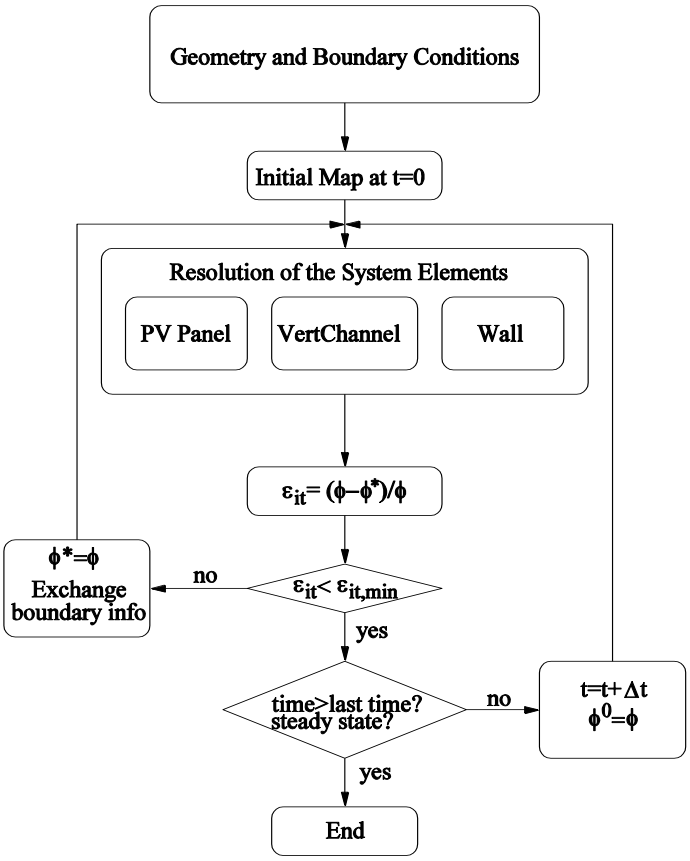

Fig. 1: Global resolution algorithm

2. Numerical Methodology

In the NEST numerical platform, the system is a collection of some basic elements. These elements can individually be solved for given boundary conditions, which are obtained from neighboring elements. This object-oriented modular platform is intended to permit efficient coupling between these elements, which, in turn, can be solved by means of different levels of modeling, like one-dimensional or two-dimensional models, simplified energy balances or CFD models based on large eddy or direct numerical simulations. For the critical elements of the façade or building, the numerical platform permits the use of the existing CFD module based on Termofluids code (Lehmkuhl et al., 2007) in order to provide high precision results, and the coupling of these with the resolution of other elements that can use different levels of modeling. The NEST numerical platform is designed to allow parallel computation, thus redistributing the computational resources according to the demands of the employed elements.

The global resolution algorithm of the numerical model is shown in Figure 1. At each iteration, once the inputs (e.g. temperature, heat flux etc.) are obtained from the neighbors, the governing equations for each element are solved and the final outputs are supplied again to the neighboring elements as boundary conditions. Iterations continue until convergence is reached at a given time step and next time step calculation starts as the variables are updated. Details of the numerical platform are explained in (Damle et al., 2011).

3. Description of the case and the implemented elements

The present work focuses on the implementation of a multi-functional ventilated façade model, which - coupled with the existing models of the NEST numerical platform- can be a useful tool to predict the thermal and fluid dynamic behavior of the façades and buildings which employ these elements. In Figure 2 the schematic view of the case under study is given. The existing building envelope is retrofitted by means of a PV panel which is installed in the façade to form a vertical ventilation channel.

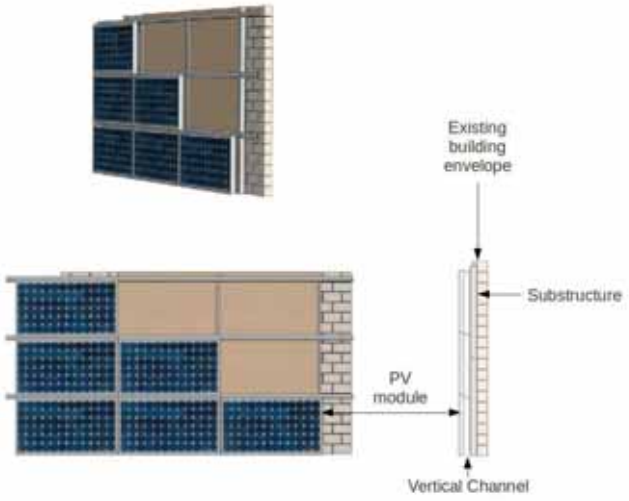

Fig. 2: Schematic view of the multi-functional ventilated façade with PV modules

The implemented multi-functional ventilated façade element is formed by linking a vertical natural convection channel element with a PV panel element and an opaque wall element on both sides as shown in Figure 3. The resulting module is designed to operate under open and closed channel modes or natural and forced convection regimes. The module also allows multi-storey channels by means of linking different channel elements vertically. Using the modularity of the numerical platform, the vertical natural convection channel element can be linked with other elements like transparent wall or electrochromic glass, thus can potentially submit to investigation numerous façade configurations using different innovative elements, and their influence on the room conditions.

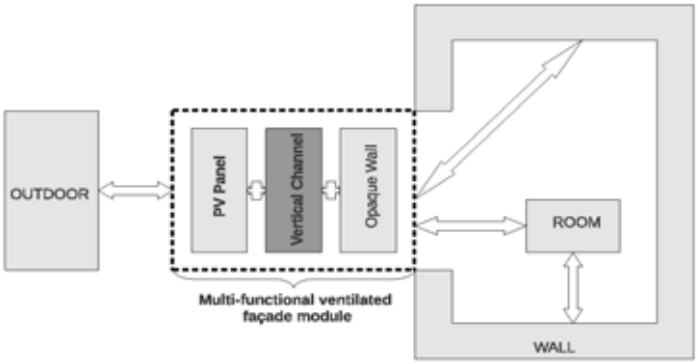

Fig. 3: Scheme of the system as a collection of elements.

3.1 PV Panel

In Figure 4 the schematic view and the geometric discretization of the PV Panel is shown. The PV Panel is modeled essentially as an opaque one dimensional conduction element with inner heat generation. The present work focuses on the thermal behavior of the façade, therefore the inner heat generation of the panel is defined as

$$Q_{PV} = (1 - \eta_{PV}) Q_s \frac{A_s}{V_{PV}} \quad \text{(eq. 1)}$$

which is then employed as a source term in the transient one dimensional conduction equation as

$$\rho\, C_p \frac{\partial T}{\partial t} = \frac{\partial}{\partial x}\left(\lambda \frac{\partial T}{\partial x}\right) + Q_{PV} \quad \text{(eq. 2)}$$

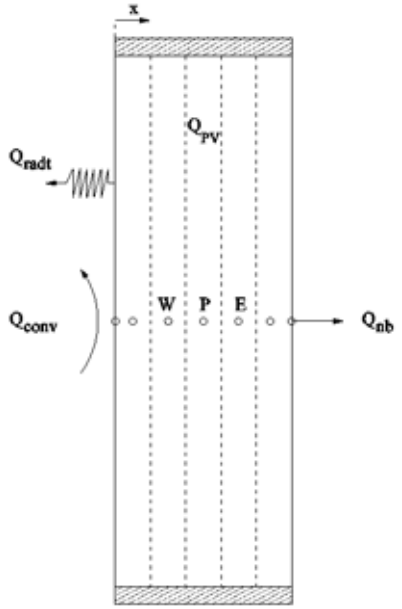

Fig. 4: Discretization of the PV Panel element. The boundary conditions represent the thermal radiation and convection heat transfer with outdoors and heat transferred to the neighboring element, Q_{nb}.

As boundary conditions, PV Panel element is expected to be linked with the existing outdoor element which provides instantaneous outdoor meteorological data. The energy balance in the boundary control volume involves convection heat transfer with outdoors, thermal radiation exchange with the sky, and conduction heat transfer in the panel. The algebraic equation in the boundary can be expressed as

$$A_P^{PV} T_P = A_E^{PV} T_E + b^{PV} \quad \text{(eqs. 3)}$$

where

$$A_P^{PV} = \lambda \frac{2A_s}{\Delta x} + \alpha_o A_s$$

$$A_E^{PV} = \lambda \frac{2A_s}{\Delta x}$$

$$b^{PV} = \alpha_o A_s - Q_{radt}$$

with $Q_{radt} = \varepsilon\sigma\left(T_w^4 - T_{sky}^4\right)$ and $T_{sky} = 0.0552\, T_{amb}^{3/2}$.

In the other boundary, the energy balance involves simply the conduction heat transfer in the PV Panel which is equal to the heat transferred to the neighboring element. If the PV Panel is linked with a vertical channel, this heat (Q_{nb} in Figure 4) is balanced with the convection heat transfer to the air in the channel.

3.2 Vertical Channel

The discretized forms of the governing equations for the air flowing through the vertical channel element are presented in this subsection. For geometric discretization see Figure 5. The channel is vertically divided into a number of control volumes (CV) homogeneously, where the nodes are located in the center of the CVs. The temperature and pressure maps are evaluated in the nodes of the centered mesh (see Figure 5, left), while the velocity field is evaluated at the faces of the centered CVs, which correspond to the center of the staggered grid as can be observed in the right hand side of the Figure 5.

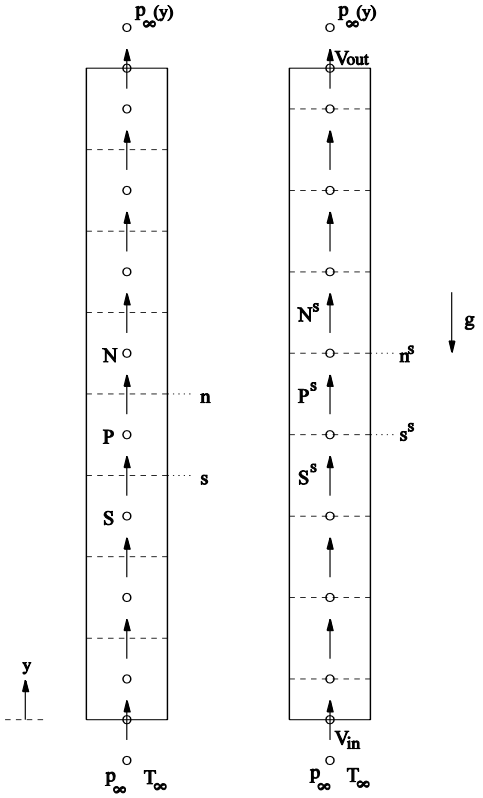

Fig. 5: Discretization of the Vertical Channel element. Centered (left) and staggered (right) grids are used for the energy and momentum equations, respectively.

3.2.1 Momentum equation

The semi-discretized form of the momentum equation can be written as

$$\frac{\partial m_P^s v_P^s}{\partial t} + \dot{m}_n^s v_n^s - \dot{m}_s^s v_S^s = (P_P - P_E)S + \left(\rho_P^s - \rho_{ref}\right)dV - \left(\frac{f_f}{4}\right) \dot{m}_P^s \frac{v_P^s}{2S} A_p \text{ (eq. 4)}$$

where superscript s indicates that the quantity is to be evaluated at the corresponding node or face of the staggered grid, and f_f is the Darcy friction factor for parallel plates as given in (Wong, 1977). Considering that the semi-discrete continuity equation at the staggered grid is given as

$$\frac{\partial m_P^s}{\partial t} + \dot{m}_n^s - \dot{m}_s^s = 0 \text{ (eq. 5)}$$

the eq. 4 can be rearranged by subtracting from it the the above semi-discrete continuity equation multiplied by v_P yielding

$$\frac{m_P^s v_P^s - m_P^{s,0} v_P^{s,0}}{\Delta t} + \dot{m}_n^s v_n^s - \dot{m}_s^s v_S^s - \left(\frac{m_P^s - m_P^{s,0}}{\Delta t} + \dot{m}_n^s - \dot{m}_s^s\right) v_p = (P_P - P_E)S + \left(\rho_P^s - \rho_{ref}\right)dV - \left(\frac{f_f}{4}\right) \dot{m}_P^s \frac{v_P^s}{2S} A_p \text{ (eq. 6)}$$

which can be discretized using an appropriate numerical scheme as explained in (Patankar, 1980).

3.2.2 Continuity equation

The conservation of mass in a centered CV of Figure 5 takes the following form

$$\frac{\rho_p dV - \rho_P^0 dV^0}{\Delta t} + \rho_n v_n S_n - \rho_s v_s S_s = 0 \text{ (eq. 7)}$$

from which a pressure correction equation can be obtained. The momentum equation cannot be solved properly unless the correct pressure field is employed, in other words an incorrect pressure field leads to an incorrect velocity field. Considering that p' is the pressure correction term, $p' = p - p^*$, and v' is the velocity correction term defined similarly as $v' = v - v^*$, these two terms can be related as

$v'_n = d_n\,(P'_P - P'_E)$ and $v'_s = d_s\,(P'_W - P'_P)$ where d_n and d_s are the SIMPLEC coefficients given as

$d_k = \frac{S_k}{A_P - (A_N + A_S)}$ (eq. 8)

with k denoting the CV face, and the coefficients A_P, A_N, A_S come from the discretized momentum equation (see Patankar 1980 for details). Due to compressibility, density correction $\rho' = \rho - \rho^*$ is necessary, which can be related to the pressure using the ideal gas relation as $\rho'_P = K\, P'_P$.

3.2.3 Energy equation

Considering a centered CV of Figure 5, the semi-discretized energy equation can be written as:

$\frac{\partial}{\partial t}[m_P(h_P + e_P)] + \dot{m}_n(h_n + e_n) - \dot{m}_s(h_s + e_s) = dV\frac{\partial p}{\partial t} + dQ_{conv}$ (eq. 9)

where dQ_{conv} is the convection heat transfer from the vertical walls of the channel to the air. Using a similar approach as is done in the momentum equation, the continuity equation multiplied by enthalpy h_P is subtracted from eq. 9 yielding

$\frac{\partial}{\partial t}[m_P(h_P + e_P)] + \dot{m}_n(h_n + e_n) - \dot{m}_s(h_s + e_s) + \left(\frac{\partial m_P}{\partial t} + \dot{m}_n - \dot{m}_s\right) h_P = dV\frac{\partial p}{\partial t} + dQ_{conv}$ (eq. 10)

An upwind numerical scheme is employed for the convection terms. The formulation is closed with

$dQ_{conv} = \sum_i \alpha \left(T_{w,i} - T_P\right) dA_i$ (eq.11)

where α for both walls is obtained from the Nusselt number (Nu) correlations in (Wong, 1977) for two parallel plates at different temperatures as a function of Grashof (Gr) and Prandtl (Pr) numbers. For laminar flow

$\overline{Nu} = 0.18(Gr\, Pr)^{\frac{1}{4}}\left(\frac{L}{w}\right)^{-\frac{1}{9}} Pr^{-\frac{1}{4}}$ (eq. 12)

For turbulent flow, i.e. for Gr numbers greater than 2×10^5, however, the expression

$\overline{Nu} = 0.065(Gr\, Pr)^{\frac{1}{3}}\left(\frac{L}{w}\right)^{-\frac{1}{9}} Pr^{-\frac{1}{3}}$ (eq. 13)

is used. Then, the convection heat transfer coefficient is calculated from $\alpha = \overline{Nu}(\lambda/L)$.

3.2.4 Boundary conditions

For the hydrodynamic boundary conditions in the vertical channel element, the Bernoulli equation is applied in the inlet of the channel, assuming acceleration from an unperturbed point at the bottom of the channel, and thus the inlet pressure is calculated as $P_{in} = P_\infty - \frac{1}{2}\rho_0 v_{in}^2$ while in the outlet the pressure is established as $P_{out} = P_\infty - \rho_o g\, L$. As for the thermal boundary conditions, the inlet temperature is set to the ambient temperature T_{amb}, while the temperature of the isothermal vertical walls of the channel are obtained from the neighboring elements.

4. Code validation

In order to validate the code, the implemented elements are separately linked with fixed value elements to form systems for which there exists an analytic solution.

PV Panel, being essentially modeled as an opaque one-dimensional conduction element, is linked with two fixed value elements, obtaining a one-dimensional plate with Dirichlet boundary conditions on both ends. In the absence of radiation, as can be seen from eq. 1, Q_{PV} is zero, for which the steady-state solution of the system reduces to a linear temperature profile in the panel. Simulating this configuration with the implemented model, the results obtained are observed to match exactly with the analytical results. Similarly, simulations of the panel using known constant internal heat generation have been carried out, obtaining the corresponding analytical results. Owing to these results, the PV Panel is considered to be validated properly.

Regarding the Vertical Channel element, the code is verified and validated by means of defining a Vertical Channel with two vertical constant temperature isothermal plates. In the special case of assigning the vertical plate temperatures equal to the Vertical Channel air inlet temperature, the air flow in the channel due to natural convection is not expected to occur since in the absence of heating or cooling there is no driving

force for the flow to take place. The numerical model effectively does not produce a flow for the configuration, which is served as a preliminary verification of the code.

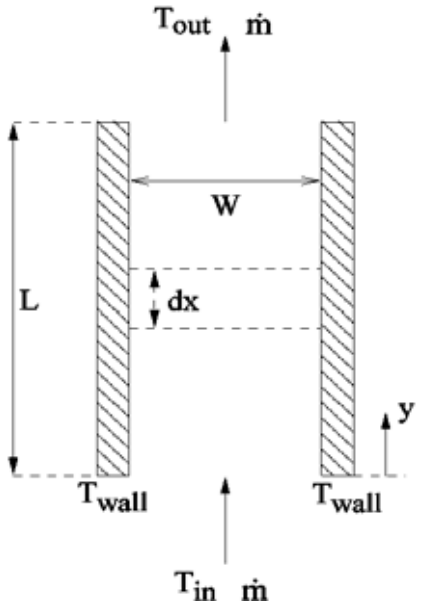

Fig. 6: Schematic view of a flow in a vertical channel.

In order to validate the code, the analytical solution presented in (Bar-Cohen and Rohsenow, 1984) is used (see Figure 6 for the schematic view of the studied case). Considering laminar, two-dimensional, fully-developed flow with constant thermophysical properties and a constant known convection heat transfer coefficient, the local bulk temperature in the channel can be obtained by means of an energy balance in the differential element as

$$T_{f,y} = T_{wall} - (T_{wall} - T_{in})e^{-\Gamma y} \quad \text{(eq. 14)}$$

Equating the pressure drop term to the buoyancy term of the momentum equation, the mass flow in the channel can be given as

$$\dot{m} = \frac{\bar{\rho}^2 g\beta W^3(\bar{T}_f - T_{in})}{12\mu} \quad \text{(eq. 15)}$$

while heat transferred to the fluid in the channel is found as

$$Q = \left[\frac{c_p\bar{\rho}^2 g\beta W^3 S}{12\mu}\,(T_{wall} - T_{in})\left(1 - \frac{1-e^{-\Gamma L}}{\Gamma L}\right)\right]\,[(T_{wall} - T_{in})(1 - e^{-\Gamma L})] \quad \text{(eq. 16)}$$

See the reference (Bar-Cohen and Rohsenow, 1984) for the details of the derivation of the above expressions. A number of simulations have been carried out using the numerical tool, and the obtained results are compared with the analytical solution in Table 1. The tested cases are for a vertical channel of aspect ratio 10, and air inlet temperature of 295 K. The results generally show good agreement with the analytical results, especially for smaller temperature differences. As for higher temperature differences, there are deviations from the analytical results up to 20 %, which can be attributed to the differences in the assumed hypotheses of the two solutions, like one-dimensional vs. two-dimensional velocity profiles, constant vs. variable thermophysical properties (consequently the use of Boussinesq approximation vs. consideration of the non-Boussinesq effects), low-Mach number effects vs. incompressible flow assumption, fully-developed vs. developing flow regimes, and differences in the boundary conditions. Notice that at smaller temperature differences, influence of these effects is expected to diminish, which accordingly leads to better agreement as can be observed in Table 1.

Tab. 1: Validation of the Vertical Channel by comparison with the analytical data

CASE	T_{wall}	Gr	α	$\dot{m}_{num}$	$\dot{m}_{ana}$	Q_{num}	Q_{ana}
I	295	0	10.0	0	0	0	0
II	300	8.9e4	2.5	8.7 e-5	8.9e-5	0.41	0.42
III	305	1.7e5	2.5	1.35e-4	1.39e-4	1.14	1.17
IV	305	1.7e5	5.0	1.65e-4	1.75e-4	1.57	1.65
V	310	2.5e5	5.0	2.13e-4	2.27e-4	2.89	3.04
VI	315	3.2e5	10.0	3.01e-4	3.35e-4	5.82	6.37
VII	315	3.2e5	15.0	3.24e-4	3.70e-4	6.48	7.32
VIII	335	5.6e5	20.0	5.09e-4	6.11e-4	20.02	23.64
IX	335	5.6e5	30.0	5.40e-4	6.75e-4	21.60	26.78

5. Preliminar façade optimization by numerical tool

Once the implemented elements are validated, the numerical tool is used to optimize a multi-functional ventilated façade like one shown in Figure 7. The façade is composed of three elements: i) an outer PV Panel, ii) air channel, iii) a composite wall formed by three layers. The thermophysical properties of the materials constituting the elements of the façade are known. All the dimensions of the elements except the width of the channel are given. Subject to the meteorological conditions of a typical day (see Figure 8, left), a parametric study of different channel widths is carried out. Consequently, the obtained results are plotted for comparison in Figures 8 to 10.

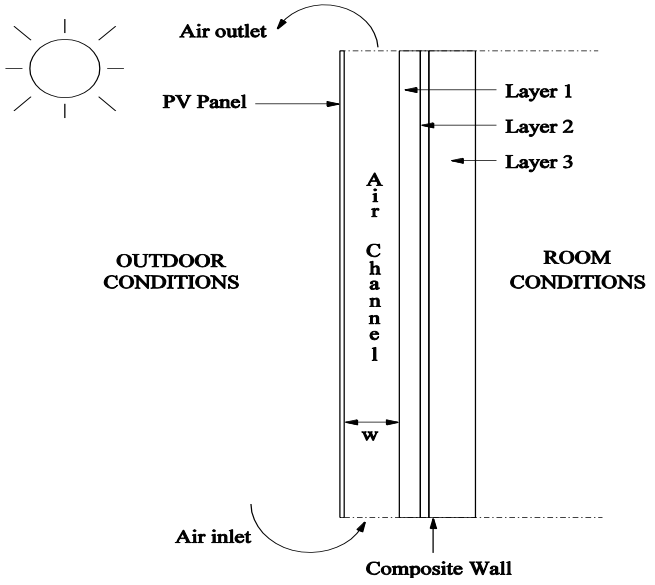

Fig. 7: Schematic view of a flow in a vertical channel.

In the mentioned figures, results corresponding to some representative channel widths are depicted. In has been concluded that a width of $w = 0.12\ m$ is the optimum channel width for the meteorological conditions and geometry under consideration. Note that for the channel widths in the extreme cases of $w = 0.03\ m$ or $w = 0.50\ m$ evacuated heat reduces considerably with respect to intermediate widths (see Figure 8, right). Although the two narrowest channel options provide highest convection heat transfer coefficients (see Figure 9, right), these geometries cause enhanced skin friction, thus reducing the mass flow drastically as can be observed in the right hand side of Figure 10, thus, in overall, these geometries result in poor performance as the evacuated heat is concerned.

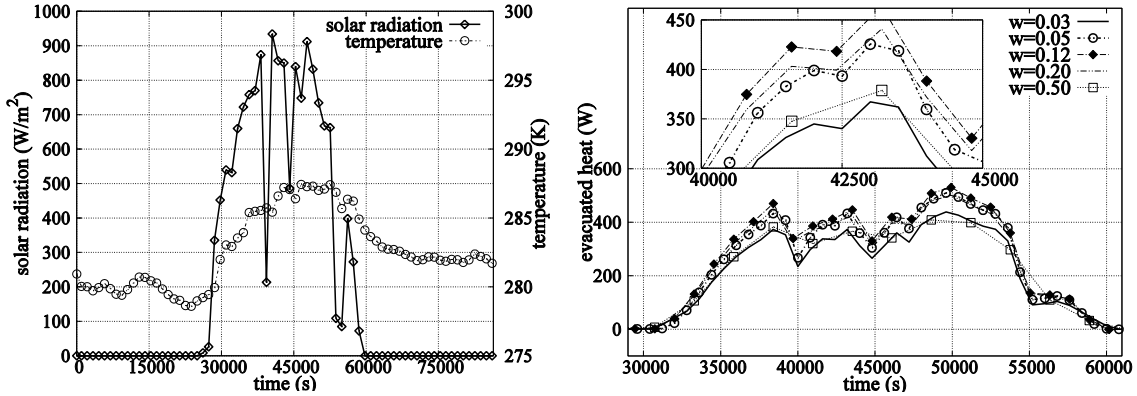

Fig. 8: Time evolution of outdoor data for the tested day (left) and the calculated evacuated heat for different widths (right).

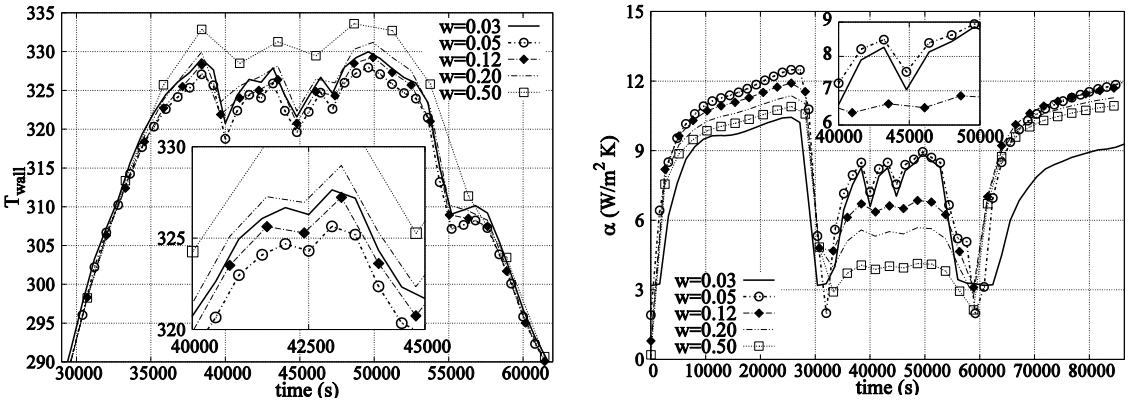

Fig. 9: Time evolution of the channel wall temperature (left) and the heat transfer coefficient (right).

The channel outlet temperatures are also depicted in Figure 10 for comparison purposes. The narrowest option naturally gives the highest outlet temperature due to reduced mass flow.

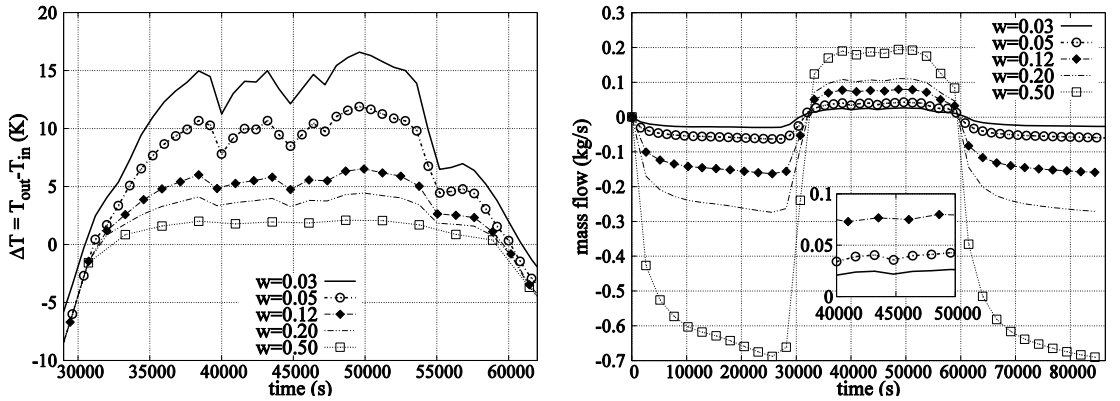

Fig. 10: Time evolution of the temperature rise (left) and mass flow (right) in the channel.

These results have shown the improved thermal performance of the $w = 0.12\,m$ option, however note that the reduction in the performance is not expected to diminish drastically as long as the deviations from this optimum width is considerably small, which can justify the selection of slightly different geometries due to the influence of other criteria like economic issues, construction ease or permitted mass flow rate, among others.

6. Conclusions

A multi-functional façade model including a PV Panel and a Vertical Channel element is implemented within an existing parallel, object-oriented numerical platform for the prediction of the thermal performance of the buildings. The implemented model is validated by means of existing analytical data. The model is intended to be a useful tool in the retrofitted building simulations, especially in configurations where innovative elements like PV panels, ventilation channels or electrochromatic devices are employed. The

numerical tool is used to optimize a typical multi-functional ventilated façade, testing different vertical channel widths and comparing the thermal performances of each configuration. The outcomes of the present work, followed by a more extensive study, are expected to be a starting point in the construction of a first generation of a real-size multi-functional façade, which in turn is seen as an indispensible tool to validate the implemented model experimentally.

Acknowledgments

This work has been financially supported by the European Community FP7 Programme, EeB.NMP.2013-3 No 609377 "RESSEEPE Project". The authors thankfully acknowledge this support.

Nomenclature

Quantity	Symbol	Unit
Ambient temperature	T_{amb}	K
Channel height	L	m
Channel width	w	m
Coefficient of thermal expansion	β	K^{-1}
Control volume width	Δx	m
Convection coefficient	α	W m^{-2} K^{-1}
Cross-section area	S	m^2
Density	ρ	kg m^{-3}
Dynamic viscosity	μ	kg m^{-1} s^{-1}
Efficiency	η	-
Emissivity	ε	-
Gas constant	K	s^2 m^{-2}
Gravity	g	m s^{-2}
Incident Solar Energy	Q_s	W m^{-2}
Lateral area	A	m^2

Quantity	Symbol	Unit
Mass flow rate	$\dot{m}$	kg s^{-1}
Pressure	p	kg m^{-1} s^{-2}
Sky temperature	T_{sky}	K
Specific enthalpy	h	J kg^{-1}
Specific heat	c	J kg^{-1} K^{-1}
Specific kinetic energy	e	J kg^{-1}
Stefan-Boltzmann constant	σ	W m^{-2} K^{-4}
Thermal conductivity	λ	W m^{-1} K^{-1}
Thermal parameter	Γ	m^{-1}
Thermal radiation flux	Q_{radt}	W m^{-2}
Time step	Δt	s
Velocity	v	m s^{-1}
Volume	V	m^3
Wall temperature	T_{wall}	K

References

Bar-Cohen, A., Rohsenow, W.M., 1984. Thermally optimum spacing of vertical, natural convection cooled, parallel plates. Journal of Heat Transfer, 126(1), pp. 116-123.

Damle, R., Lehmkuhl, O., Golomer, G., Rodríguez, I., 2011. Energy Simulation of Buildings with an Object-Oriented Tool. In Proceedings of the ISES Solar World Congress, Kassel, Germany.

Lehmkuhl, O., Pérez-Segarra, C.D., Borrell, R., Soria, M., Oliva, A., 2007.TERMOFLUIDS: A new Parallel unstructured CFD code for the simulation of turbulent industrial problems on low cost PC cluster. In Proceedings of the Parallel CFD 2007 Conference, pp. 1–8.

Patankar, S.V., 1980. Numerical Heat Transfer and Fluid Flow, Hemisphere Publishing Corporation.

Pérez-Lombard, L., Ortiz, J., Pout, C., 2008. A review on buildings energy consumption information. Energy and Buildings, 40, pp. 394-398.

Wong, H.Y., 1977. Handbook of Essential Formulae and Data on Heat Transfer for Engineers, Longman.